

# Modeling Extreme Mass Ratio Inspirals within the Effective-One-Body Approach

Nicolás Yunes,<sup>1</sup> Alessandra Buonanno,<sup>2</sup> Scott A. Hughes,<sup>3</sup> M. Coleman Miller,<sup>4</sup> and Yi Pan<sup>2</sup>

<sup>1</sup>*Department of Physics, Princeton University, Princeton, NJ 08544, USA.*

<sup>2</sup>*Maryland Center for Fundamental Physics, Department of Physics,  
University of Maryland, College Park, MD 20742, USA.*

<sup>3</sup>*Department of Physics and MIT Kavli Institute,  
77 Massachusetts Avenue, Cambridge, MA 02139, USA.*

<sup>4</sup>*Maryland Astronomy Center for Theory and Computation,  
Department of Astronomy, University of Maryland, College Park, MD 20742, USA.*

We present the first models of extreme-mass-ratio inspirals within the effective-one-body (EOB) formalism, focusing on quasi-circular orbits into non-rotating black holes. We show that the phase difference and (Newtonian normalized) amplitude difference between EOB and Teukolsky-based gravitational waveforms can be reduced to  $\lesssim 10^{-1}$  rads and  $\lesssim 2 \times 10^{-3}$ , respectively, after a 2-year evolution. The inclusion of post-Newtonian self-force terms in the EOB approach leads to a phase disagreement of  $\sim 6$ –27 rads after a 2-year evolution. Such inclusion could also allow for the EOB modeling of waveforms from intermediate-mass ratio, quasi-circular inspirals.

*Introduction.* Extreme mass ratio inspirals (EMRIs) are the gravitational wave (GW) driven coalescences of stellar mass compact objects with supermassive black holes (SMBHs). When the large BH's mass is in the range  $10^5 M_\odot - 10^7 M_\odot$ , EMRI waves are emitted at frequencies well suited to measurement by the planned *Laser Interferometer Space Antenna* (LISA). Because EMRI events are expected to be abundant [1] and will carry detailed information about strong-field spacetimes near SMBHs [2], they are high-priority targets for LISA observation. The intrinsic febleness of these waves will require accurate waveform templates to detect and faithfully measure the signals produced by Nature. Because EMRI waves arise from very strong field motions near the SMBH's innermost stable circular orbit (ISCO), traditional post-Newtonian expansions are not well suited to modeling their signals; the binary's orbital speed  $v/c \sim 0.1 - 0.5$ , a regime where traditional post-Newtonian techniques perform poorly. Numerical models built using black hole (BH) perturbation theory should be able to reliably model EMRI signals. However, the computational cost of covering the full span of EMRI parameter space (including effects due to BH spin, orbital inclination, and eccentricity) is likely to be very high [1].

This has motivated us to examine techniques for reliably approximating these waves at a much smaller computational cost. The effective-one-body (EOB) formalism was introduced as a way to analytically describe the inspiral, merger, and ringdown waves emitted by comparable-mass BH binaries [3, 4]. This formalism was then extended to higher post-Newtonian (PN) orders [5], spinning BHs [6, 7], small mass-ratio mergers [8], and was further improved by introducing factorized waveforms [8, 9]. By calibrating a few adjustable parameters in the EOB-dynamics and waveforms, [10, 11] showed that the phase and amplitude of the EOB and numerical-relativity waveforms can be made to agree within the numerical error of the simulations, thus providing GW de-

tectors with faithful templates. In this analysis, we now consider calibrating EOB with BH perturbation theory in order to model EMRI waves.

As a first step, we restrict our models to a small compact object spiraling along a quasi-circular orbit into a non-spinning SMBH [12]. Although the assumptions of circularity and zero spin can and will be relaxed in the future, there exist astrophysical motivations for this initial choice of binary configuration. For example, the tidal separation scenario for EMRIs [13] implies nearly circular but arbitrarily inclined orbits in the  $> 10^{-4}$  Hz frequency band relevant for LISA, and the accretion disk capture picture [14] implies orbits that are both nearly circular and in the spin plane of the SMBH. In addition, the characteristics of the SMBHs themselves are uncertain in the  $< 10^7 M_\odot$  mass range most relevant for LISA. In some astrophysical scenarios, the growth of these BHs is dominated by the accretion of stars moving on random trajectories, instead of by the accretion of gas disks, thought to be more important for higher-mass SMBHs [15]. Such growth would lead to  $\hat{a} \equiv |\vec{J}|/M^2 \ll 1$  (in natural units with  $G = c = 1$ , which we use throughout this paper), hence the Schwarzschild (nonrotating) spacetime is a reasonable first approximation.

We now systematically compare EMRI waveforms computed in the EOB approach to those calculated using BH perturbation theory via solution of the Teukolsky equation [16, 17]. As we describe in the remainder of this *Letter*, we find that appropriately calibrated EOB waveforms in fact do an excellent job modeling waves computed using BH perturbation theory. This suggests that EOB is very likely to be an outstanding tool for modeling EMRI waves in future LISA data analysis.

*Analytical and Numerical Modeling.* For a BH binary with masses  $m_1$  and  $m_2$ , we set  $M = m_1 + m_2$  and  $\mu = m_1 m_2 / M = \nu M$ . In absence of spins, the motion is constrained to a plane. Introducing dimensionless polar coordinates  $(r, \Phi)$  (where  $r$  is  $M$ -normalized)

and their reduced ( $\mu$ -normalized) conjugate momenta  $(p_r, p_\Phi)$ , the non-spinning EOB Hamiltonian reads [3]  $H^{\text{real}} = M \sqrt{1 + 2\nu [(H^{\text{eff}} - \mu)/\mu]} - M$ . The effective Hamiltonian here is [3, 5, 8]

$$H^{\text{eff}} = \mu \sqrt{p_{r_*}^2 + A(r) \left[ 1 + \frac{p_\Phi^2}{r^2} + 2(4 - 3\nu)\nu \frac{p_{r_*}^4}{r^2} \right]}, \quad (1)$$

where  $p_{r_*}$  is the reduced conjugate momentum to the EOB *tortoise* radial coordinate  $r_*$ , and  $A(r)$  and  $D(r)$  are Padé-resummed functions, which can be read from Eqs. (54) and (59) in [18]. The EOB Hamilton equations are written in terms of the reduced (i.e., dimensionless) quantities  $\hat{H}^{\text{real}} \equiv H^{\text{real}}/\mu$ ,  $\hat{t} = t/M$  [4]:

$$\frac{dr}{d\hat{t}} = \frac{A(r)}{\sqrt{D(r)}} \frac{\partial \hat{H}^{\text{real}}}{\partial p_{r_*}}, \quad \frac{d\Phi}{d\hat{t}} = \frac{\partial \hat{H}^{\text{real}}}{\partial p_\Phi}, \quad (2)$$

$$\frac{dp_{r_*}}{d\hat{t}} = -\frac{A(r)}{\sqrt{D(r)}} \frac{\partial \hat{H}^{\text{real}}}{\partial r}, \quad \frac{dp_\Phi}{d\hat{t}} = \hat{\mathcal{F}}_\Phi. \quad (3)$$

Initial data for these equations is obtained through a mock evolution, which is initialized at an initial orbital separation of  $100M$  using post-circular initial conditions [4]. Having the EOB inspiral dynamics in hand, we compute the multipole-decomposed GW  $h_{\ell m}$ , where  $\ell$  and  $m$  refer to spherical harmonics. We use the factorized waveforms of [9]

$$h_{\ell m} = h_{\ell m}^{(N, \epsilon)} \hat{S}_{\text{eff}}^{(\epsilon)} T_{\ell m} e^{i\delta_{\ell m}} (\rho_{\ell m})^\ell, \quad (4)$$

where  $h_{\ell m}^{(N, \epsilon)}$  is the Newtonian contribution given in Eq. (4) of [9],  $\epsilon = 0$  (or 1) for  $\ell + m$  even (or odd),  $\hat{S}_{\text{eff}}^{(\epsilon)}$ ,  $T_{\ell m}$ ,  $\delta_{\ell m}$  and  $\rho_{\ell m}$  can be read from Eqs. (15)–(25) and (C1)–(C6) in [9]. The EOB GW phase is computed by solving  $\dot{\Phi}_{\ell m} = -(1/m) \text{Im}[\dot{h}_{\ell m}/h_{\ell m}]$ . Errors in the EOB waveforms arise due to inaccuracies in the numerical solution of the Hamilton equations (2) and (3), and inaccurate initial data. We have investigated all such sources of error and estimate them to be no worse than  $\delta\Phi_{22} \lesssim 0.03$  rads in the waveform's phase and  $\delta h_{22}/h_{22} \lesssim 10^{-7}$  in the normalized amplitude after a 2-year evolution. This cumulative error is primarily dominated by the accuracy of the routine used in `Mathematica` to solve (2) and (3).

As described above, we compare these waves with waveforms computed from the Teukolsky equation. We used the code described in [16] (modified to use the spectral techniques described in [19]) to construct the Newman-Penrose curvature scalar  $\psi_4$ . In the distant radiation zone, this is simply related to the GWs carried from the system:  $\psi_4 \rightarrow 1/2(\dot{h}_+ - i\dot{h}_\times)$  as  $r \rightarrow \infty$ . Similarly, one can show that  $\psi_4$  near the event horizon describes tidal interactions of the BH with the orbiting body [20]. Our code works in the frequency domain, decomposing  $\psi_4$  into harmonics and multipoles by  $\psi_4 = R^{-1} \sum_{\ell m} Z_{\ell m} {}_{-2}Y^{\ell m}(\theta, \phi) e^{-im\omega t}$  where  ${}_{-2}Y^{\ell m}(\theta, \phi)$  is

a spin-weight  $-2$  spherical harmonic, and  $\omega = \sqrt{M/r^3}$  is the frequency of circular Schwarzschild orbits. The amplitude  $Z_{\ell m}$  is found by first constructing a Green's function to the radial Teukolsky equation,

$$(r^2 - 2Mr)^2 \frac{d}{dr} \left( \frac{1}{r^2 - 2Mr} \frac{dR_{\ell m}}{dr} \right) - V_{\ell m}(r) R_{\ell m} = 0, \quad (5)$$

and then integrating that Green's function over a source made from the stress-energy tensor of the small body orbiting the BH; see [16] for details of that source and the potential appearing in Eq. (5). One detail worth emphasizing is that there are two asymptotic solutions to Eq. (5) which are of particular physical interest. One describes radiation that is purely outgoing as  $r \rightarrow \infty$ ; it is from this solution that we construct the flux of radiation to infinity, and the waveform that distant observers measure. The other is purely ingoing on the BH's event horizon, and describes the tidal interaction of the orbiting body with the BH.

Once  $\psi_4$  has been constructed, it is simple to extract the flux of energy carried by radiation and absorbed by the BH. The flux to infinity is given by

$$\left( \frac{dE}{dt} \right)^\infty = \sum_{\ell m} \frac{|Z_{\ell m}|^2}{4\pi m^2 \omega^2}; \quad (6)$$

a similar (but somewhat more complicated) sum describes absorption by the BH. Once these quantities are computed, we calculate the rate at which the orbital radius changes,  $\dot{r}$ , by noting that for slow backreaction the system evolves through a sequence of geodesic orbits.

We construct the  $\psi_4$  solution on a discrete grid of orbits from  $r = 10,000M$  to the Schwarzschild ISCO at  $r = 6M$  (in Boyer-Lindquist coordinates), evenly spacing our orbits in  $v \equiv \sqrt{M/r}$ . (Since stable circular orbits do not exist for  $r < 6M$ , we cannot infer  $\dot{r}$  from  $dE/dt$  in this regime.) Errors in the Teukolsky-based waveforms are primarily due to truncation of the sums over  $\ell$  and  $m$ , and due to discretization in orbital phase space (apart from the intrinsic numerical precision of the Teukolsky code, which is roughly  $10^{-14}$ ). The sums are taken until they have converged to a fractional error of no more than  $10^{-10}$  [16, 17]. In the low velocity region  $v < 0.1$ , however, we find in practice that the flux is accurate to at least  $10^{-13}$ . Phase space discretization error arises because the fluxes are cubic-spline interpolated from a discrete adiabatic sequence of geodesic orbits. We find that a discretization of 1,000 points over the range  $v \in [0.01, 0.408]$  is sufficiently fine to guarantee an accuracy no worse than  $10^{-2}$  rads in the GW phase after a 2-year evolution.

*Systems, Regions and Models.* To demonstrate the flexibility of the EOB model in matching the Teukolsky-based waveforms, we examine two fiducial EMRI systems, labeled system-I and system-II, that sample different regions of the LISA noise curve. In both cases,

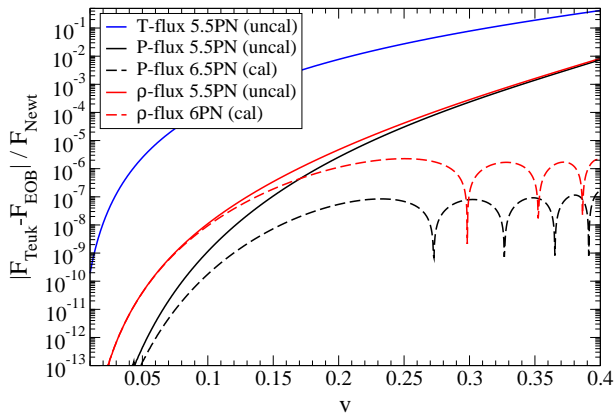


FIG. 1: Absolute value of the difference in the Newtonian normalized Teukolsky and EOB fluxes as a function of orbital velocity. Calibrating the Padé or  $\rho$ -flux improves the agreement by orders of magnitude at the orbital speeds of BHs close to the ISCO.

we consider a 2-year long quasi-circular inspiral of non-spinning BHs. System-I has  $(m_1, m_2) = (10^5, 10)M_\odot$ ; system-II has  $(m_1, m_2) = (10^6, 10)M_\odot$ . We do not consider lower or higher total mass binaries as they would either reach the ISCO outside the LISA optimal sensitivity band (LISA’s noise raises sharply above  $\sim 10^{-2}$  Hz) or lie inside the white-dwarf confusion limit (below  $\sim 0.003$  Hz [21]). System-II ( $m_2/m_1 = 10^{-5}$ ) begins at an initial separation  $r_{\text{in}} \simeq 10.6M$  and terminates at the ISCO, sweeping GW frequencies in the range  $f_{\text{GW}} \in [1.8 \times 10^{-3}, 4.4 \times 10^{-3}]$  Hz. System-I ( $m_2/m_1 = 10^{-4}$ ) starts at  $r_{\text{in}} \simeq 29.34M$  and terminates at  $r_{\text{fin}} \simeq 16.1M$ , sweeping frequencies in the range  $f_{\text{GW}} \in [4 \times 10^{-3}, 10^{-2}]$  Hz. These choices allow the study of the early and late EMRI dynamics, while guaranteeing the GW signal is in the sensitive part of the LISA band.

We define two EOB models differing in the resummation of the tangential radiation-reaction force in Eq. (3). Using the balance equation we can write  $\widehat{\mathcal{F}}_\Phi = -F/(\nu\Omega)$  where  $F$  is the GW energy flux. We use (i) the Padé-approximant to the energy flux [11, 22]  $F^{\text{P}} = F_q^p(v_{\text{pole}})$ , where  $v_{\text{pole}}$  is an adjustable parameter locating the EOB light-ring, and  $p+q$  is twice the approximant’s PN order [i.e.,  $(v/c)^{(p+q)}$ ], and (ii) the  $\rho$ -approximant to the energy flux [9]  $F^\rho = 2/(16\pi) \sum_{\ell=2}^{\ell=8} \sum_{m=1}^{m=\ell} (m\Omega)^2 |Rh_{\ell m}|^2$ , where  $h_{\ell m}$ ’s are given by Eq. (4). Except when investigating the effect of the self-force, the orbital dynamics are always computed setting  $\nu = 0$  in  $A(r)$  and  $D(r)$ , i.e., for a Schwarzschild BH. Similarly, we set  $\nu = 0$  in the radiation-reaction force except for its overall  $\nu$ -dependence.

*Results.* Figure 1 shows the absolute value of the difference between the Newtonian-normalized ( $F_{\text{Newt}} = 32\nu^2 v^{10}/5$ ) Teukolsky and EOB (*uncalibrated* and *calibrated*) fluxes as a function of the orbital velocity  $v$ . The Teukolsky flux includes energy both radiated to infinity and absorbed by the BH’s event horizon. The uncalibrated Padé-flux ( $F_4^{\text{P}}$ ) and  $\rho$ -flux are computed

through 5.5PN order, but in the Padé flux we also add horizon absorption corrections [23] and set  $v_{\text{pole}}$  to the Schwarzschild light-ring value. The uncalibrated Taylor-flux (i.e., the PN Taylor-expanded flux [18]) gives a residual at least two orders of magnitude worse than the uncalibrated Padé and  $\rho$  fluxes. The calibrated Padé-flux ( $F_6^{\text{P}}$ ) is computed through 6.5PN order, including the horizon absorption corrections, and calibrating  $v_{\text{pole}}$  and the 6PN and 6.5PN coefficients [ $v_{\text{pole}} = 0.54834$ ,  $\mathcal{F}_{12} = 5152.53 - 1015.94 \log(16v^2)$ , and  $\mathcal{F}_{13} = -12053.6 + 774.703 \log(16v^2)$ ; see, e.g., Eq. (19)-(40) in [18]]. The calibrated  $\rho$ -flux is computed through 6PN order, without horizon absorption corrections, and calibrating the 6PN coefficients in  $\rho_{22}$  [ $c_6^{\rho_{22}} = 640.6 - 453.7 \text{eulerlog}_2(v^2)$ ] and the 5PN coefficients in  $\rho_{33}$  [ $c_5^{\rho_{33}} = -918.3 + 679.7 \text{eulerlog}_2(v^2)$ ] (see Eq. (47) in [9]). For velocities  $v \in [0.01, 0.1]$  the agreement is better than  $10^{-8}$  with a best agreement of  $10^{-13}$  near  $v = 0.01$  for all models.

Comparisons of Teukolsky-based and EOB waveforms are performed once they are aligned in time and phase. We perform such alignment by minimizing the statistic in Eq. (23) of [11], which is equivalent to maximizing the fitting factor over time and phase of coalescence in a matched filtering calculation with white noise [11]. The alignment procedure depends rather sensitively on the alignment window chosen. We choose to align the waveforms in the low-frequency regime, i.e., in the interval  $t \in [0, 64]\lambda_{\text{GW}}$ , where  $\lambda_{\text{GW}}$  is the GW wavelength,  $t \simeq (0, 0.006M)$  [ $t \simeq (0, 0.013M)$ ] months for system-I [system-II], to a level of  $10^{-10}$  [ $10^{-6}$ ] rads in the phase for systems-I [system-II]. We have checked that choosing any interval window of width  $< 2^9\lambda_{\text{GW}}$  changes the final dephasing by less than  $10^{-3}$  rads and the relative amplitude difference by less than  $10^{-6}$ .

In the left panel of Fig. 2 we plot the absolute value of the phase difference, or *dephasing*, between the dominant  $h_{22}$  mode of the Teukolsky-based and EOB waveforms as a function of time in units of months. We find that after 2-years the dephasing is  $\sim 40$  (3000) rads for system-I (system-II) when using the EOB-model with Taylor-flux [18], a result in qualitative agreement with previous investigations [24]. The EOB model with uncalibrated Padé-flux at 5.5PN has a dephasing of  $\sim 5$  (530) rads for system-I (system-II), which can be reduced to  $\sim 0.1$  (0.01) rads if we employ the calibrated Padé-flux at 6.5PN. The EOB model with uncalibrated  $\rho$ -flux at 5.5PN has a dephasing of  $\sim 10$  (530) rads for system-I (system-II), which can be reduced to  $\sim 2$  (0.8) rads if we consider the calibrated  $\rho$ -flux at 6PN. In the right panel of Fig. 2, we compare the amplitude of the dominant mode  $A_{22} = |h_{22}|$ , computed in the EOB and Teukolsky frameworks. After 2-years of evolution, both the calibrated Padé- and  $\rho$ -flux EOB models have a disagreement of  $\sim 10^{-5}$  for system-I and  $\sim 2 \times 10^{-4}$  for system-II. Such a phase and amplitude agreement is fantastic when

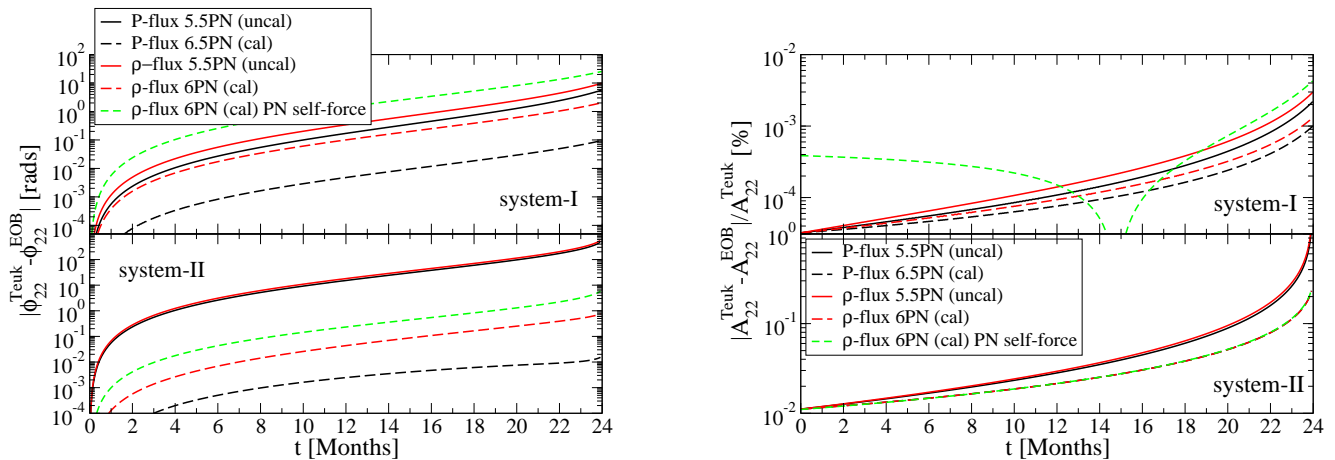


FIG. 2: Absolute value of the dephasing (left) and fractional amplitude difference (right) of the dominant GW (2, 2) mode as a function of time in months. Again, with the introduction of calibrated higher-order terms, the differences are small even over a full two year coherent integration.

one takes into account the 2-year length of observation, during which the binary of system-I (system-II) evolves over  $\sim 2 \times 10^6$  ( $\sim 9 \times 10^5$ ) rads. Quite interestingly, we find that if we switch on the relative  $\nu$  terms in the 3PN EOB Hamiltonian Eq. (1) (conservative self-force) and in the flux (dissipative self-force) the dephasing, for the EOB-model with  $\rho$ -flux at 6PN, increases to  $\sim 27$  (6) rads for system-I (system-II), while the Newtonian normalized amplitude difference increases to  $4 \times 10^{-4}$  ( $2.5 \times 10^{-3}$ ) for system-I (system-II). We notice that the main effect comes from the dissipative self-force, a result consistent with [25] for circular orbits.

We also compare the strongest higher harmonics using the EOB model with Padé-flux at 6.5PN. In the case of the  $(\ell, m) = (3, 3)$  and  $(\ell, m) = (4, 4)$  modes we find dephasings of  $\sim 0.14$  (0.07) and  $\sim 0.18$  (0.09) rads, and normalized amplitude differences of  $\sim 6 \times 10^{-5}$  ( $4 \times 10^{-3}$ ) and  $\sim 3 \times 10^{-4}$  ( $9 \times 10^{-3}$ ), for system-I (system-II). These dephasings are comparable to those found for the  $(\ell, m) = (2, 2)$  mode because in both frameworks the GW phase (and frequency) can be computed directly from the orbital phase (and frequency), up to errors of less than  $\sim 1$  rad over a 2-year integration. As a consequence, the above comparisons are almost entirely governed by the trajectories of the test particle. Finally, we find that higher harmonics contribute significantly less to the signal-to-noise ratio relative to the (2, 2) mode. In particular, we computed the signal-to-noise ratio averaged over beam-pattern functions with a noise spectral density that includes white-dwarf confusion noise. Including up to  $\ell = 5$  ( $\ell = 7$ ) for system-I (system-II) guarantees a recovery of 97% of the total signal-to-noise ratio, with the  $\ell = m$  modes the most dominant.

*Data Analysis Implications and Discussion.* The above results have demonstrated that the EOB framework can be used to model EMRIs for LISA data analysis purposes, with the advantage of allowing for the consistent

inclusion of both dissipative and conservative PN self-force terms. In addition, such terms allow the construction of waveforms from intermediate-mass ratio inspirals, where first-order BH perturbation theory is expected to fail. The comparisons made here, however, serve only as a proof-of-principle, as one must now generalize the formalism to more generic spinning EMRIs, and more complicated orbital geometries.

Lastly, the EOB framework allows us to provide for the first time a metric-based estimate of the number of templates needed for EMRI systems in LISA data analysis. We construct the metric of the template submanifold [26] following the prescription of [22]. For a 2-month evolution, we estimate that one requires less than  $10^7$  EOB templates to cover the template bank with a minimal match of 0.97 in the total mass range ( $10^5$ – $10^6$ ) $M_\odot$  and mass ratio range ( $10^{-4}$ – $10^{-5}$ ).

*Acknowledgments.* We are grateful to Frans Pretorius and Eric Poisson for useful suggestions and comments, and to William Throwe for computational assistance. NY, AB and YP, and SAH acknowledge support from the NSF grants PHY-0745779, PHY-0603762 and PHY-0903631, PHY-0449884; AB, SAH and MCM also acknowledge support from NASA grants NNX09AI81G, NNX08AL42G and NNX08AH29G.

- 
- [1] J. R. Gair, L. Barack, T. Creighton, C. Cutler, S. L. Larson, E. S. Phinney, and M. Vallisneri, *Classical and Quantum Gravity* **21**, 1595 (2004).
  - [2] S. A. Hughes, *AIP Conf. Proc.* **873**, 233 (2006), gr-qc/0608140.
  - [3] A. Buonanno and T. Damour, *Phys. Rev.* **D59**, 084006 (1999).
  - [4] A. Buonanno and T. Damour, *Phys. Rev.* **D62**, 064015 (2000).
  - [5] T. Damour, P. Jaranowski, and G. Schaefer, *Phys. Rev.*

- D62**, 084011 (2000).
- [6] T. Damour, Phys. Rev. **D64**, 124013 (2001).
  - [7] A. Buonanno, Y. Chen, and T. Damour, Phys. Rev. **D74**, 104005 (2006).
  - [8] T. Damour and A. Nagar, Phys. Rev. **D76**, 064028 (2007).
  - [9] T. Damour, B. R. Iyer, and A. Nagar, Phys. Rev. **D79**, 064004 (2009).
  - [10] T. Damour and A. Nagar, Phys. Rev. **D79**, 081503 (2009).
  - [11] A. Buonanno et al., Phys. Rev. **D79**, 124028 (2009).
  - [12] P. Amaro-Seoane et al., Class. Quantum Grav. **24**, 113 (2007).
  - [13] M. C. Miller et al., ApJ Letters **631**, L117 (2005).
  - [14] D. Syer, C. J. Clarke, and M. J. Rees, Mon. Not. R. Astron. Soc. **250**, 505 (1991).
  - [15] J. Wang and D. Merritt, ApJ **600**, 149 (2004).
  - [16] S. A. Hughes, Phys. Rev. **D61**, 084004 (2000).
  - [17] S. A. Hughes, Phys. Rev. **D64**, 064004 (2001).
  - [18] M. Boyle et al., Phys. Rev. **D78**, 104020 (2008).
  - [19] R. Fujita and H. Tagoshi, Prog. Theor. Phys. **113**, 1165 (2005).
  - [20] S. A. Teukolsky, Astrophys. J. **185**, 635 (1973).
  - [21] A. J. Farmer and E. S. Phinney, Mon. Not. Roy. Astron. Soc. **346**, 1197 (2003).
  - [22] T. Damour, B. R. Iyer, and B. S. Sathyaprakash, Phys. Rev. **D57**, 885 (1998).
  - [23] Y. Mino et al., Prog. Theor. Phys. Suppl. **128**, 1 (1997).
  - [24] I. Mandel and J. R. Gair, Class. Quant. Grav. **26**, 094036 (2009).
  - [25] A. Pound and E. Poisson, Phys. Rev. **D77**, 044013 (2008).
  - [26] B. J. Owen, Phys. Rev. **D53**, 6749 (1996).